electronics

MDPI

Article

Module Tester for Positron Emission Tomography and Particle Physics

David Baranyai [1], Stefan Oniga [2,3], Balazs Gyongyosi [1], Balazs Ujvari [1,4,*] and Attia Mohamed [5,6]

[1] Department of Data Science and Visualization, Faculty of Informatics, University of Debrecen, 4032 Debrecen, Hungary; divaldo@mailbox.unideb.hu (D.B.); gyongyosi.balazs@science.unideb.hu (B.G.)
[2] Department of IT Systems and Networks, Faculty of Informatics, University of Debrecen, 4032 Debrecen, Hungary; oniga.istvan@inf.unideb.hu
[3] Department of Electric, Electronic and Computer Engineering, Technical University of Cluj-Napoca, North University Center of Baia Mare, 430083 Baia Mare, Romania
[4] HUN-REN Institute for Nuclear Research, 4026 Debrecen, Hungary
[5] Physics Department, Faculty of Science, Zagazig University, Zagazig 44519, Egypt; attiamohamed@mailbox.unideb.hu
[6] Doctoral School of Physics, University of Debrecen, 4032 Debrecen, Hungary
* Correspondence: ujvari.balazs@inf.unideb.hu

Abstract: The combination of high-density, high-time-resolution inorganic scintillation crystals such as Lutetium Yttrium Oxyorthosilicate (LYSO), Yttrium Orthosilicate (YSO) and Bismuth Germanate (BGO) with Silicon Photomultiplier (SiPM) sensors is widely employed in medical imaging, particularly in Positron Emission Tomography (PET), as well as in modern particle physics detectors for precisely timing sub-detectors and calorimeters. During the assembly of each module, following individual component testing, the crystals and SiPMs are bonded together using optical glue and enclosed in a light-tight, temperature-controlled cooling box. After integration with the readout electronics, the bonding is initially tested. The final readout electronics typically comprise Application-Specific Integrated Circuits (ASICs) or low-power Analog-to-Digital Converters (ADCs) and amplifiers, designed not to heat up the temperature-sensitive SiPM sensors. However, these setups are not optimal for testing the optical bonding. Specific setups were developed to test the LYSO + SiPM modules that are already bonded but not enclosed in a box. Through large data collection, small deviations in bonding can be detected if the SiPMs and LYSOs have been thoroughly tested before our measurement. The Monte Carlo simulations we used to study how parameters—which are difficult to measure in the laboratory (LYSO absorption length, refractive index of the coating)—affect the final result. Our setups for particle physics and PET applications are already in use by research institutes and industrial partners.

Keywords: SiPM; FPGA; PET; particle physics

Citation: Baranyai, D.; Oniga, S.; Gyongyosi, B.; Ujvari, B.; Mohamed, A. Module Tester for Positron Emission Tomography and Particle Physics. *Electronics* **2024**, *13*, 3066. https://doi.org/10.3390/electronics13153066

Academic Editor: Daniela Isidori

Received: 20 June 2024
Revised: 16 July 2024
Accepted: 24 July 2024
Published: 2 August 2024

1. Introduction

Medical imaging devices, specifically Positron Emission Tomography (PET) or large detectors for experimental particle physics, are designed, mounted and operated using similar methodologies. The components are selected and assembled according to the expected operating conditions of the detector, and the parts are tested at each important stage of the construction. The crystal and Silicon Photomultiplier (SiPM), selected and then glued together based on factory or custom calibrations, is called a module. At this stage, the bonding can be tested with calibrated radiation sources. The final readout electronics are optimised for the final operation of the detector, pose limitations for this testing and can only be used after proper cooling, mechanical protection and boxing of the whole device. If the calibration, with this readout electronics, finds a fault in the gluing, it will be a long process to repair it.

High-speed and high-precision setups were developed that can test the modules of the Lutetium Yttrium Oxyorthosilicate (LYSO) (other types of scintillators can also be tested) and SiPM-based detectors without their own readout electronics. The module is connected to the electronics in a light-tight box, and the quality of the bonding is checked using the measured spectrum of a calibrated radiation source. One of the typical defects is an air bubble trapped in the adhesive during gluing, which can be determined by the displacement of the photopeak in the spectrum. Another defect is the inhomogeneity of the thickness of the glue, which can be measured by the ratio of the photopeak positions of the neighbouring crystals. This study shows how bond testing is possible using measurements and simulations. The most extensive user of this development in the near future will be the CERN CMS BTL (Compact Muon Solenoid at CERN, Barrel Timing Layer) sub-detector [1,2] and the BNL (Brookhaven National Laboratory in New York) ePIC collaboration [3] at the EIC [4] (Electron Ion Collider) accelerator.

The first SiPM upgrade at CMS is the replacement of Avalanche Photodiodes (APDs) with SiPMs for part of (Hadron Calorimeter) an HCAL [5]; to improve performance, SiPMs allow significantly higher gain and better Photon Detection Efficiency (PDE). The increased gain delivers robust electrical signals that mitigate the impact of electrical noise and enable signal splitting for time-to-digital converter (TDC) measurements. Additionally, their enhanced effective quantum efficiency and capability to detect single photoelectrons significantly improves the energy resolution, calibration and monitoring of the calorimeters. The T2K experiment was the first in particle physics to extensively utilise SiPMs (56,000 sensors) [6]. At CERN, the CALICE Analog Hadron Calorimeter (AHCAL), which began operating in 2006, was the first detector to use a large number of SiPMs (7608 sensors) [7]. At the sPHENIX, 20,000 SiPMs were tested, at CMS BTL, 350,000 SiPMs will be tested, and at ePIC, probably in the order of 1 million sensors and their detectors are to be tested. It can be seen that the number of SiPM-based detectors in particle physics is growing rapidly and their accuracy requires testing more accurately than the factory values, which must be checked several times throughout the detector's construction. Similar assumptions can be made for medical imaging; if the accuracy of image reconstruction is limited by the approximate knowledge of the sensor parameters, similar testing steps can be expected and hundreds of millions of sensors are already in use in this industry today. A mass tester is expected to be necessary for the assembly of various detectors and medical instruments.

2. Module Tester

2.1. SiPM Sensors

SiPMs are advanced solid-state sensors that combine the advantages of traditional PMTs with the robustness and compactness of semiconductor devices used in photon detection applications. These sensors offer high sensitivity to single photons, making them ideal for low-light detection scenarios. SiPMs consist of a matrix of tiny silicon APDs and offer exceptional timing precision, often in the range of tens of picoseconds. SiPMs provide high internal gain (typically in the range of 10^6) due to the avalanche multiplication process within each microcell. It is insensitive to magnetic fields and makes PET inserts suitable for use inside MRI scanners. One of the main applications, other than those mentioned above, is that of Light Detection and Ranging (LIDAR) systems, which are important, for example, in autonomous vehicles. In medicine and high-energy physics, two parameters are important:

1. Breakdown voltage refers to the voltage at which the silicon APDs within the SiPM enter Geiger mode, initiating the avalanche multiplication process. It is a critical parameter as it determines the operational voltage range of the SiPM and influences its sensitivity and noise characteristics. Because with the predecessor of SiPMs PMT used high voltage (thousands of Volts), the operating voltage is still called HV, although it is typically around 30–60 V.

2. Gain represents the amplification factor of the SiPM, indicating how many electron–hole pairs are generated per incident photon. It is typically expressed as the ratio of output charge (in photoelectrons) to input charge (number of incident photons).

S15408 PROTO TYPE 25UM sensors are used for this test. This sensor array was developed for CMS BTL. It has 16 SiPMs (similar to Hamamtsu MPPC S13360/S13362 series (https://www.hamamatsu.com/jp/en/product/optical-sensors/mppc/mppc_mppc-array.html (accessed on 31 July 2024))) on a carrier, and the outputs are led out on the flex cable shown on the left of Figure 1. The breakdown voltage is between 38 and 40 V, and the gain at 3 V overvoltage is 2×10^5.

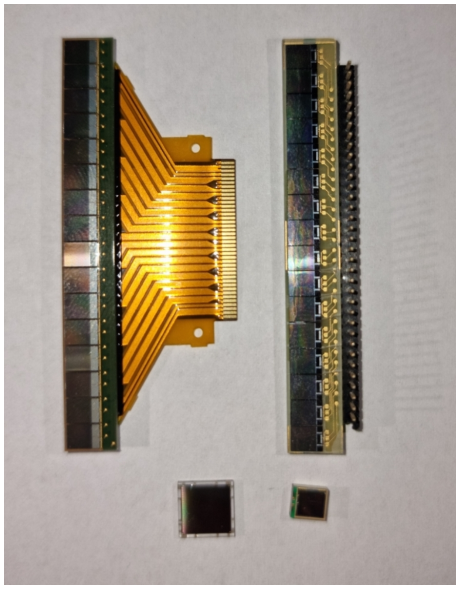

Figure 1. SiPMs with different sizes and connectors.

2.2. CMS BTL Tester

The digitizer card (Figure 2) consists of two main parts, a self-designed and developed Printed Circuit Board (PCB) with 3 ADCs and a Field-Programmable Gate Array (FPGA) card. The TVP7002 ADC (https://www.ti.com/product/TVP7002 (accessed on 31 July 2024)), designed for video applications, is a 3-channel, 8/10 bit ADC with variable readout frequency from 110 to 165 Megasamples Per Second (MSPS) designed by Texas Instruments. In this card, it is used with 10 bits and 125 MSPS. The TVP7002 features three digitizing channels, each with independent control over clamping, gain and offset. It provides an 8-bit programmable gain control and 1024-step programmable offset control, and it supports 20-bit 4:2:2 outputs with embedded syncs.

The self-developed PCB is equipped with appropriate input protection and an output level converter from 3.3 V to 1.5 V to the RAM connectors. In addition to its power supply units, it is equipped with per-channel calibration circuits and reference ICs.

The FPGA card is the Simplivity Omnicube 510-000003 server accelerator card (https://www.hpe.com/psnow/doc/a00057986enw (accessed on 31 July 2024)). It is designed to enhance the performance of SimpliVity's OmniCube systems, which are known for their hyper-converged infrastructure solutions. This card integrates storage, computing and networking functionalities into a single, scalable unit. The RAM pins are used to read out the ADCs, with 10-bit parallel buses per ADC channel (90 buses), 1 clock per ADC and a few additional buses for I2C for calibration.

The DAQ (data acquisition) (ADC + FPGA) card was installed in a small PC. The hit frequencies from the radioactive sources are about 250 kHz to 1 MHz, 8 SiPMs are measured in parallel, there are 64 ADC values, 10 bits, stored in 2 Bytes, and the total size of the raw data for 1 M hits is as follows (about 1-10s measurement, depending on the trigger conditions for a 1 MHz hit frequency): 10^6 (hits) $\times$ 64 (ADC values)$\times$ 2 Byte (for one ADC

value) × 8 (channels), which is a few GBytes of raw data. The measured ADC values are moved in the PC's memory in 32 kByte blocks per channel, from where the Root [8] framework processes and writes the 64 samples as waveforms in its own file format. Root provides efficient compression and user-friendly data processing.

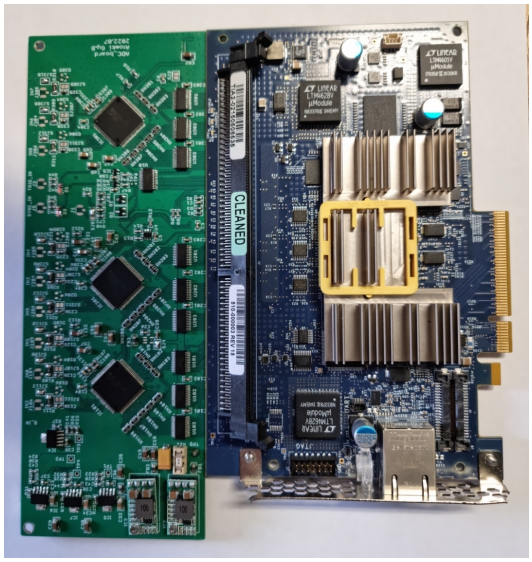

Figure 2. DAQ card.

When using a radioactive source, or a mixture of sources, with multiple gamma emitters with well-separated energies, the breakdown voltage can also be determined by varying the HV; the accuracy of this breakdown voltage depends on the accuracy and stability of the dedicated power supply (about 10 mV) and how accurately we can measure the signal integral of many photons.

In order to be able to test the already-bonded crystal and SiPMs with radioactive sources, two similar data acquisition setups were developed. The bonding of the modules takes place in several locations; the first setup is installed at the location where the bonding technique is optimised, where only a few modules are bonded per day, and the second setup is to support mass testing. The two installations differ only in the number of channels. The amplifiers, data acquisition cards and data processing methods are the same. The first unit, capable of measuring up to 8 channels in parallel, can be seen in Figure 3, and the second, where 32 channels are expected to be measured in parallel, is a server rack-mountable DAQ module (see Figure 4a). Each DAQ module can read out 16 channels, depending the size of the rack, and more channels can be measured in parallel. In this setup (see Figure 4b), 4 modules, with 8 SiPMs per module, can be measured. The measurements are analysed offline after the data taking, where another blade server with near-real-time processing will also be available.

The SiPM arrays are connected to the readout unit via Panasonic AYF534035 connectors. DG409 multiplexers distribute the SiPM output between the amplifier channels. Two ADA4807, low-noise, rail-to-rail input/output, voltage feedback amplifiers are used, and the total amplification in this setup is 13. The last stage on this board is the AD8014 low-power amplifier, which has very good drive capability for signals on 50 Ω. Series-terminated lines are used at the DAQ card as input lines. The PT1000 temperature sensor on the array is read out with ADS122U04. The front-ends can be seen with and without the modules in Figure 5b.

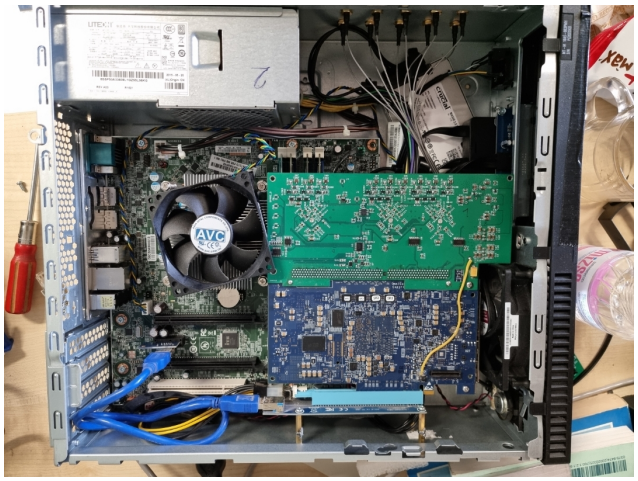

Figure 3. DAQ PC.

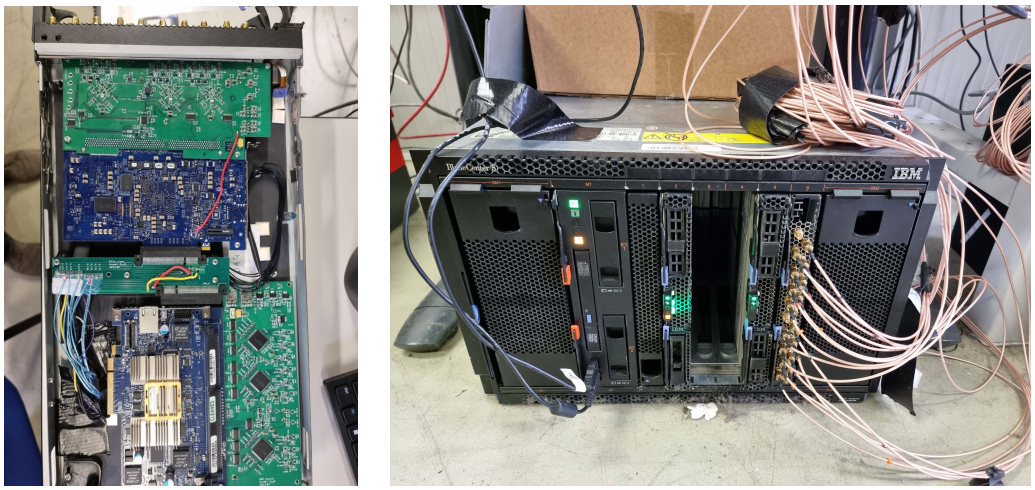

(**a**) DAQ module. (**b**) IBM server.

Figure 4. DAQ server.

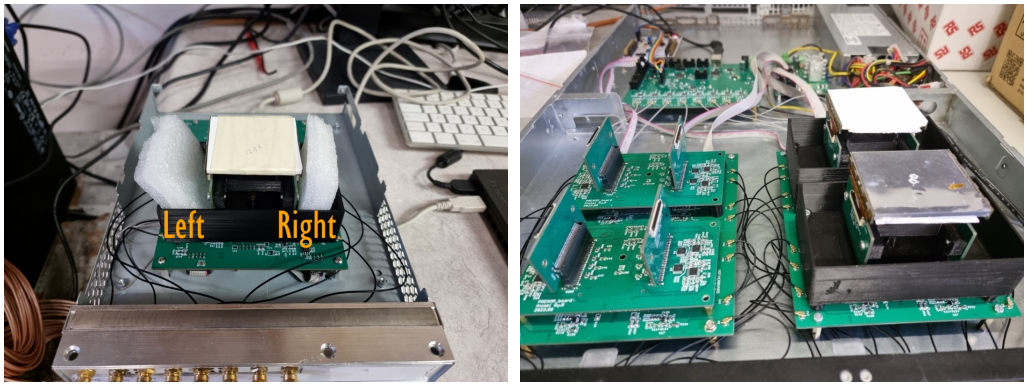

(**a**) One module. (**b**) Four modules.

Figure 5. FE.

2.3. Backend

The data acquisition board driver and readout software are available from Linux. The methods of the readout software, written in C++ (https://github.com/divaldo95/LibDAQDevice.git (accessed on 31 July 2024)), which can be used to start a measurement, are now available as a shared library, allowing the backend to communicate directly with the device (https://github.com/divaldo95/SiPMNIMeasurement (accessed on 31 July 2024)), without the need to implement interprocess communication and solve other problems that

this entails. After measurement, the data are automatically analysed using the analysis software developed in the CERN Root framework, which is also available as a separate module (shared library) (https://github.com/divaldo95/LibRootIVAnalysis (accessed on 31 July 2024)).

2.4. GUI

The user interface (Figure 6) can be accessed from any device (smartphone, tablet, laptop) and allows us to start a new measurement or monitor an existing measurement (https://github.com/divaldo95/SiPMTesterInterface (accessed on 31 July 2024)). When starting a new measurement, it is possible to select the SiPM sensor pairs to be tested one by one and to use different settings per sensor pair, for example, to set the number of data to be collected. After pressing the Start button, the testing of the selected SiPM sensors starts and the process can be monitored in the automatically updated interface. As soon as the testing of a sensor is completed, the result and evaluation are displayed in an interactive graph on the interface.

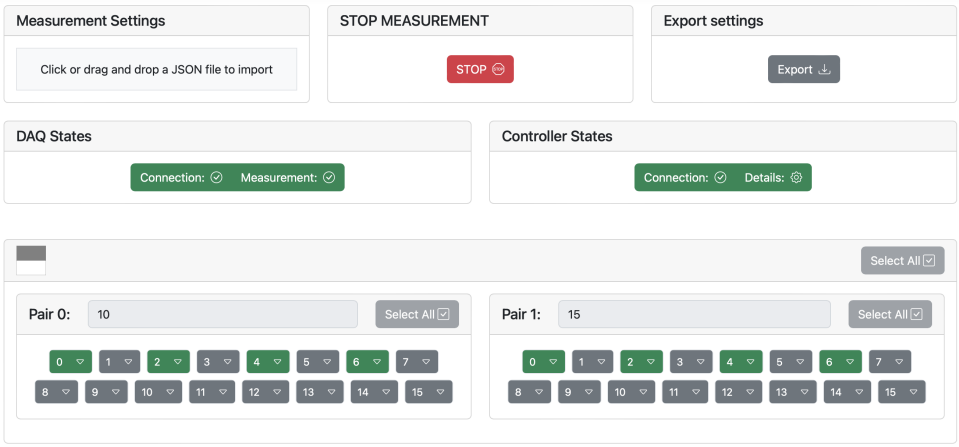

Figure 6. SiPM tester user interface.

3. Measurements

By placing Cs-137 sources (100 kBq-1 MBq) above the module (see Figure 7a), the gamma interacts with the LYSO material and produces visible photons. The number of photons is proportional to the energy deposit. The number of photons are converted to electrons by the SiPM (one photon creates about 2×10^5 electrons), the electrons appear as a short-current pulse at the output of the SiPMs, and the integral of the pulse is proportional to the energy deposit. An operational amplifier converts currents into voltage, measured by the ADC. Some of the ADC pulses can be seen in Figure 8, and their integrals are the measurable quantity that is proportional to the energy deposit in the crystal. The waveforms and the signals are offset, because the ADC measures in the range 0–1 V, but that noise can have negative values and sometimes the SiPMs undershoots. These undershoots cannot be seen if, for the analogue 0–1 V range, we use the digital 0–1023 range. Before ADC sampling, a small positive analogue value is added to the signal to prevent noise from driving the signal into negative, offsetting the ADC values by about 100; these values are removed before the integral of the signal. Since the Cs-137 isotope has one dominant 662 keV gamma, the full energy deposit can be measured by the photopeak position. Since the light yield of the LYSO crystal is about 33k photons/1000 keV [9], the photonpeak, the total energy release, produces roughly 21k visible photons; these are measured on the two ends of the module by the SiPMs. The integrated ADC value is energy-equivalent (see Figure 7b) within the statistical fluctuation of the process. Compton background is a flat distribution at lower values (Figure 7b), was not used in this calculation.

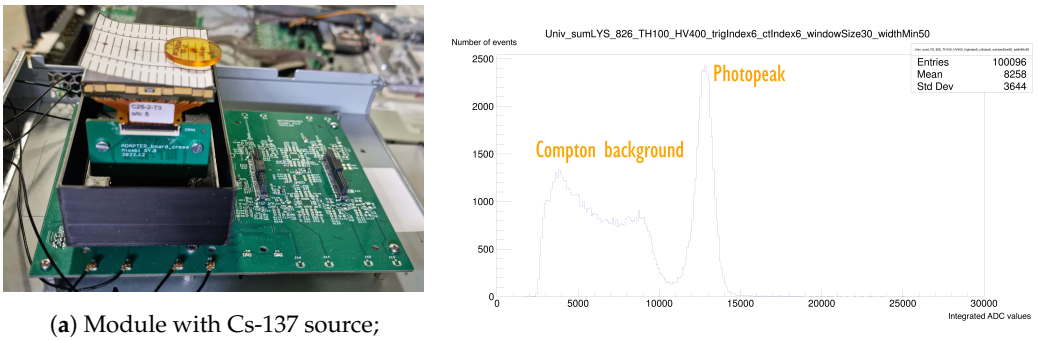

(**a**) Module with Cs-137 source; during the measurements, the source is moved along the module.

(**b**) Cs-137 spectrum, where the Compton background and photopeak are clearly distinguishable.

Figure 7. Measurements.

The SiPM Photon Detection Efficiency is about 40%. If the 21k photons created in the photopeak are evenly distributed, the sum of 4400 (21k/2 × 0.4) photon-induced electrical responses is detected by the ADC. A total of 10 sample signals can be seen in Figure 8. The first 128 ADC units are measured on the left and the second 128 ADC values at the same time on the right part of the module (see Figure 5a). One of the 16 crystals was measured using 1M samples. The trigger condition is as follows: the previous 64 ADC values from the buffer and the following 64 ones are read out if the ADC value (left or right) exceeds the threshold of 100. By integrating the peaks in the sample and plotting the sum of the left and right peak integrals, the spectrum can be obtained (Figure 7b).

Figure 8. For 10 saved inputs, the two opposite SiPM signals are shown and the triggering condition is indicated by the orange line.

3.1. Photopeak Position

With an array, 1M hits are detected and saved for every crystal. With this setup, data can be recorded from eight SiPMs simultaneously under different trigger conditions. In this measurement, the goal is to reconstruct the Cs-137 spectrum from the energy emitted in a LYSO. To avoid cross-talk, only non-adjacent SiPMs are measured, as can be seen in Figure 9a. Samples are saved when the signal of one of the SiPMs at the two ends of a LYSO goes above the threshold (Figure 8). The samples are integrated from the beginning of the peak using a window of 30 ADC units; the integrals and the spectrum can be obtained for every (16 per module) LYSO + 2 SiPM detector units. Plotting the mean and its standard deviation of the Gaussian fit of the 16 photopeaks (see Figure 9b), differences are observed between the photopeak positions of the 16 measurements. These can come from the following:

1. Different breakdown voltages and PDEs of the opposite sensors. A detailed test of the SiPMs is a must to minimise this differences.
2. Different geometries of the LYSO crystal are tested (https://indico.cern.ch/event/1091653/contributions/4592080/attachments/2347379/4003069/MTD_Poster.pdf (accessed on 31 July 2024)).
3. The reflective index of the coating and quantity of the gluing can be estimated with this measurement and simulations.

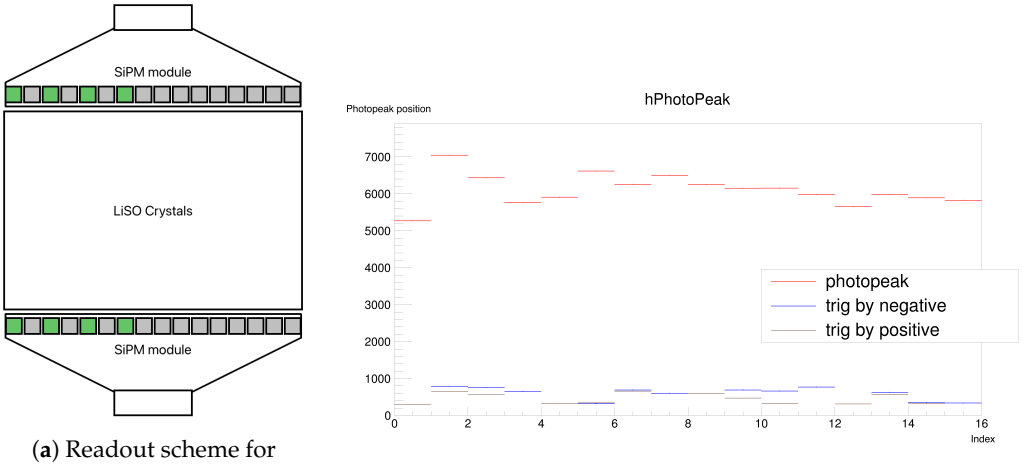

(**a**) Readout scheme for photopeak position.

(**b**) Photopeak position of an array.

Figure 9. Measurement #1.

In Figure 9b, red lines represent the photopeak positions. The blue and brown lines are also photopeak positions but with different trigger conditions. The 'trig by negative' trigger fires if the signal in any of the SiPMs of the given LYSO (say, number 6) are above the threshold, but the negative neighbour (LYSO number 5) has higher amplitude signals, meaning the gamma is detected in the LYSO number 5, but due to the optical cross-talk, optical photons from this hit are also detected in LYSO number 6, but at lower ADC integrals (around 500–1000 instead of 5000–7000).

The photopeaks are fitted with Gauss, and the sigma/mean are plotted for one module in the Figure 10. This relative width contains the uncertainty of the optical photon production and of the SiPM gain and the uncertainty of the DAQ. Based on this, the sensitivity of our method is roughly 5–10%, and changes beyond this are no longer measurable due to the uncertainty of our measurements.

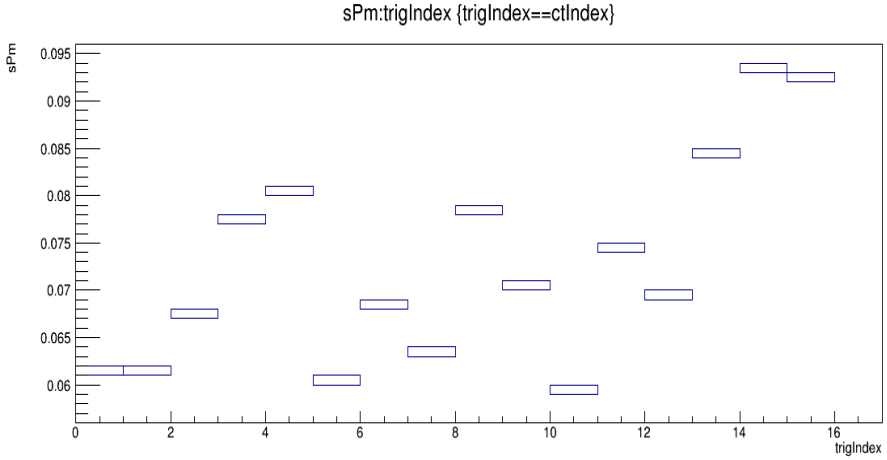

Figure 10. Sigma per mean from the measurements, 6–10%, in 16 positions was measured and fit the photopeak position.

3.2. Optical Cross-Talk

In this readout mode (Figure 11a), 4-4 adjacent SiPMs and 4 LYSOs are read out, and all eight signals are saved if the ADC value exceeds 100 at any SiPM of the eight. This method can be used to measure the cross-talk due to gluing. From the previous measurements, the integral of the photopeak can be measured. If the integral of one crystal, measured with its two SiPMs, is in this range, the integrals of the two neighbouring SiPMs are also calculated. This ratio is the cross-talk, the proportion of photons that are scattered from the first crystal through the bonding in the second crystal. The photopeak positions can be seen in red in Figure 9b, and the blues and the browns are the photopeaks on the left and right (named negative and positive according to the index of the SiPMs in the array). The shape of the spectrum can be resolved not only in the first but also in the second neighbour as a photopeak and a Compton background. The cross-talk is about 10–15% if there is a hit in the first crystal with an integral ADC value of about 8000 and at the same time close to 1000 integrated ADC values appear in the second one in the left or right neighbours. Even in the second neighbour, about 3% appears. The high integral value ensures neighbours that the hit in the photopeak was definitely in the first crystal, and the frequency of the hits minimises the chance that another hit (in the photopeak or in the Compton background) occurred in the second crystal.

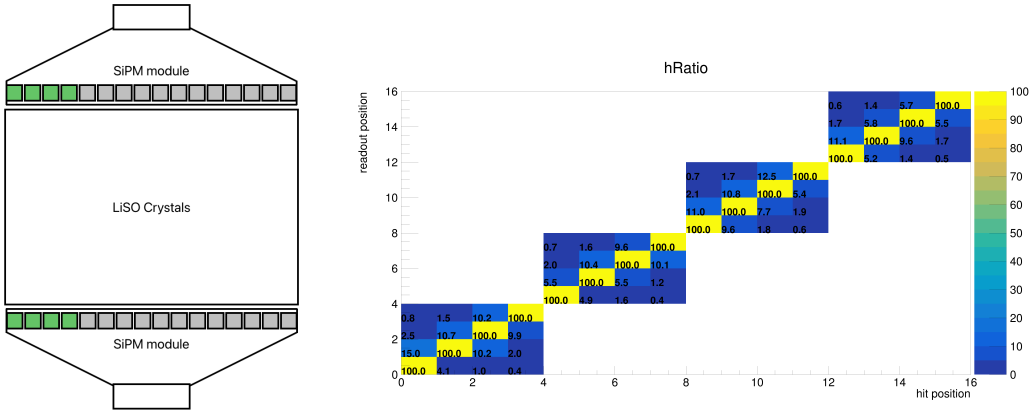

(**a**) Readout scheme for cross-talk.

(**b**) Cross-talk result; the percentage of photons detected in a given LYSO is relative to a diagonal value.

Figure 11. Measurement #2.

By recording one million hits per LYSO + 2 SiPMs and preliminary testing the SiPM gain at the given operating voltage and performing optical tests of the crystal to measure the absorption length and the refractive index, respectively, the quality control of the bonding can be performed from the position of the photopeaks and the magnitude of the cross-talk. The exact methodology is still under development; the number of hits will depend on the accuracy of SiPM and LYSO tests.

4. GEANT4 Simulation of the Module

4.1. GEANT4 Simulation

GEANT4 (Geometry ANd Tracking, fourth edition) is a versatile simulation toolkit in C++ based on object-oriented programming (OOP) [10]. It features particle tracking, geometry handling, physics models and hit recording. GEANT4 encompasses electromagnetic, hadronic and optical processes, with a library of particles, materials and elements. Its main goal is to simulate particle paths, their interactions with materials and field effects using the Monte Carlo method. GEANT4's modular structure is organised into domains with subdomains in a unidirectional flow. Essential domains include the following: Geometry and Materials, Particle Interactions with Matter, Tracking Management, Digitisation and Hit Management, Event and Track Management, Visualisation and Visualisation Framework and User Interface. The GEANT4 toolkit allows users to create complex geometric

models with various shapes and materials. It enables the definition of 'sensitive' elements that capture crucial information (hits) necessary for simulating detector responses (digitisation). Primary particles for events can be generated from both internal and external sources. GEANT4 includes a wide array of physics processes to accurately simulate particle behavior, offering users the flexibility to choose from existing methods, modify them or develop new ones. Moreover, users can interact with the toolkit via multiple (graphical) user interfaces, which facilitate the visualisation of geometry and particle tracks through various graphics systems via a well-defined interface. This interface can be customised to integrate with other systems according to user preferences. The toolkit's classes are designed to be reusable and compact, making it easy for users to extend or modify their functionalities for specific applications [11]. LYSO crystals and SiPM sensors used in particle physics [12] were simulated in this study because of the large amount of measurement data available for these. The LYSO crystal used in the simulation has the following parameters: a refractive index of 1.81, a density of 3.67 g/cm^3, a light yield of 33,200 ph/MeV, an absorption length of 10 m and a decay time of 36 ns. By changing the parameters in the simulation, it is possible to check whether the previous tests of SiPM and LYSO validate the measurements of the modules. This requires simulation results that are comparable to the measurements, including realistic modelling of the electronics.

4.2. Cs-137 Spectrum from Simulation

A simulation was performed of gamma rays emitted from Cs-137 with an energy of 662 keV hitting a LYSO crystal. The LYSO crystal is configured in a bar-like geometry with dimensions of $3 \times 3 \times 53$ mm^3. The crystal is read out by a pair of SiPMs, each with dimensions of $3 \times 3 \times 3$ mm^3, positioned at each end, as depicted in Figure 12. In this figure, the light yield is only about 1% of the original (320 instead of 33,200 ph/MeV) to show the optical photon tracks. The Cs-137 source is put on the top surface of the LYSO crystal at a position 1.5 mm along the y-axis and 26.5 mm along the z-axis. The LYSO crystal is surrounded by a thin coating layer with a reflective index of 0.999.

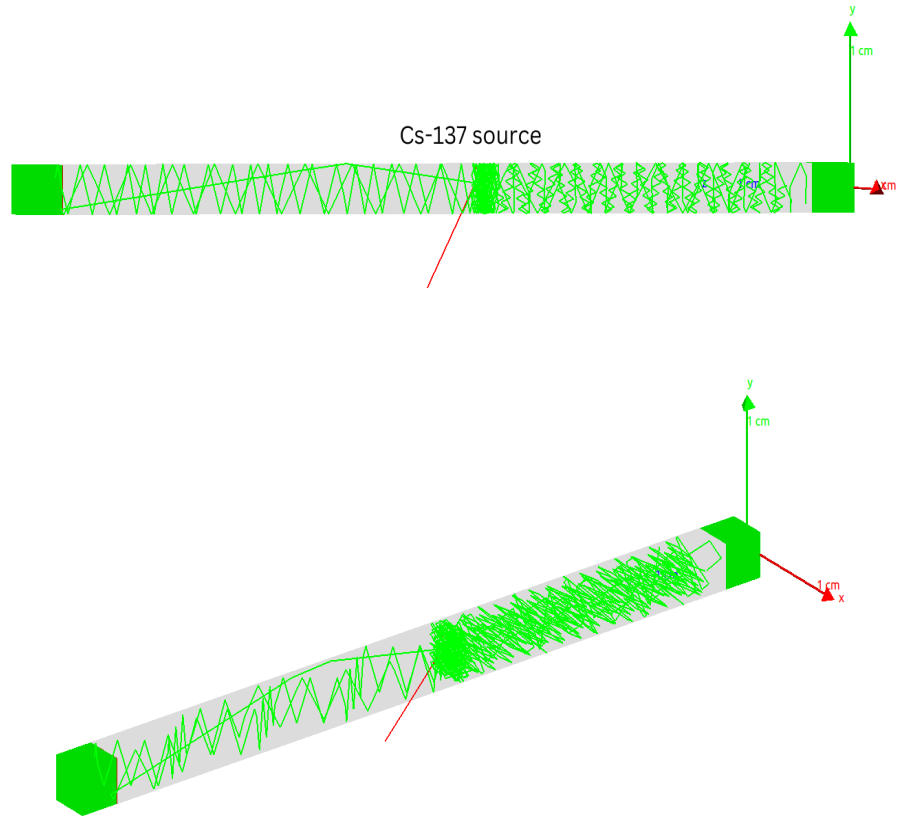

Figure 12. Geant4 schematic view of LYSO crystal with double-ended SiPM readout.

As mentioned in Section 3, the acquisition process involves measuring 128 ADC units from both the left and right SiPMs for each gamma photon hit on LYSO. To exclude waveforms with low ADC values, where the shape of the signal depends more on the noise of the electronics, a threshold of ADC $>$ 600 is applied. Linear fitting is used for the rising edges of the waveforms from both SiPMs, while exponential fitting is applied to the falling edges, as shown in Figure 13. In a given LYSO + 2 SiPM configuration, the Compton background and the photopeak are well identified in the spectrum (Figure 7b). The simulation can be compared with the measurements if a model is created for the electrical response of the optical photons detected by the SiPM. These figures clearly show that the SiPM signals in an incoming photon range have a similar shape, only the amplitude varies and the leading and falling edges are similar functions. The electrical response per photon is given by using a threshold of 600 to select the signals associated with a good-quality photon peak, by describing the shape of these signals in general and dividing by the average number of optical photons associated with the photon peak obtained in the simulation. A total of 178,733 signals from the left SiPM and 133,752 from the right SiPM, each with a threshold greater than 600, were collected and fitted. The results were filled into histograms, and these distributions were used in simulations to reconstruct the signal and the spectrum for comparison with the measurements. The slopes of the rising edges for the left and right SiPMs are depicted in Figure 14a,b, respectively. Additionally, the slopes of the exponential falling edges are illustrated in Figure 15a for the left SiPM and Figure 15b for the right SiPM.

To construct the waveform of a single optical photon from the SiPMs, we randomly select values from the distributions of the rising edge (Figure 14) and the falling edge (Figure 15) of the left and the right SiPMs. These values are used to form ADC waveforms that simulate those obtained from measurements. Subsequently, a scaling process is applied to normalise both SiPM waveforms, illustrated in Figure 16. Using GEANT4 simulation, we determine the number of photons detected by each SiPM. Based on the photon counts recorded by the left and right SiPMs in the simulation, the waveform of a single optical photon is iterated. For instance, if x photons are detected by the left SiPM and y photons by the right SiPM, the waveform of a single optical photon is repeated x times for the left SiPM and y times for the right SiPM. The resulting waveforms, combining these iterations, are shown in Figure 17, followed by calculating the integral of these simulated waveforms within the ADC window of [45, 75] units for both the left and right SiPMs. The sum of these integrals from the left and right SiPMs is then used to populate the Cs-137 spectrum in terms of ADC values, as illustrated in Figure 18. Comparing the relative width of the photopeak obtained from the simulation and our measurements, see Figure 10, it can be seen in the simulation that the error of the integral of the simulated waveforms of the gamma interaction, where the maximum number of optical photons created (photopeak) is overestimated, using amplitude-dependent fitting with finer resolution, will be the next step.

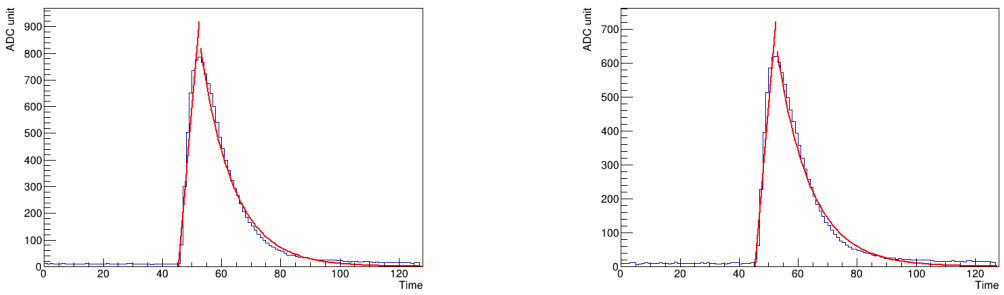

(**a**) Left SiPM (**b**) Right SiPM

Figure 13. ADC waveform for left and right SiPM with ADC amplitude threshold of >600. The blue color represents the ADC waveform, while the red color represents linear fitting for the rising edge and exponential fitting for the falling edge in both left and right SiPM.

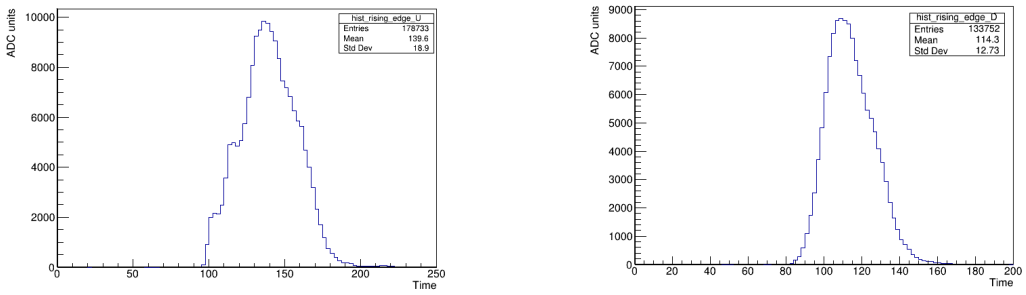

(**a**) Left. (**b**) Right.

Figure 14. Slopes from linear fitting of left and right waveforms.

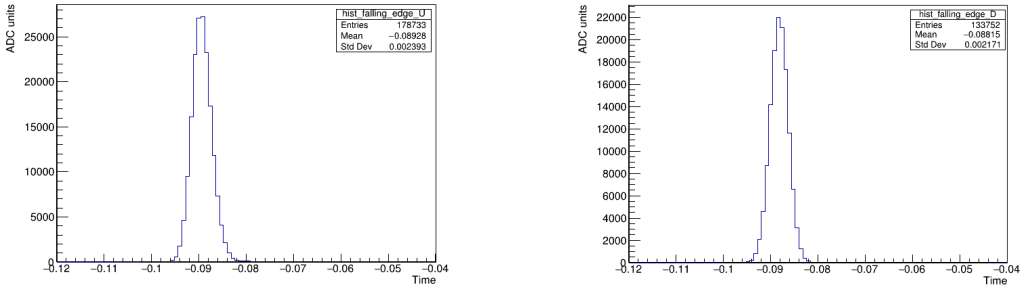

(**a**) Left. (**b**) Right.

Figure 15. Slopes from exponential fitting of left and right waveforms.

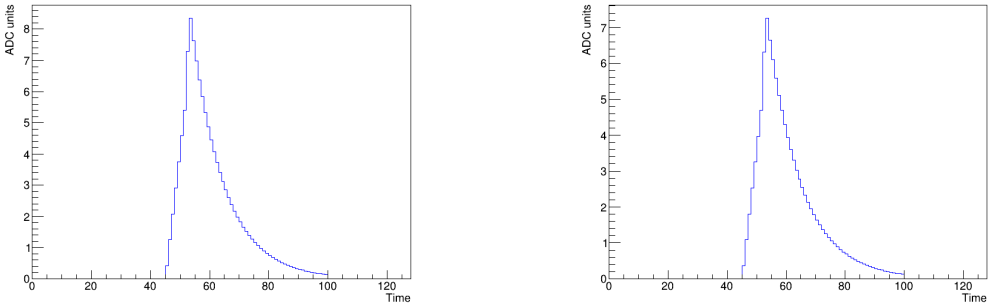

(**a**) Left SiPM. (**b**) Right SiPM.

Figure 16. Left and right single optical photon waveforms.

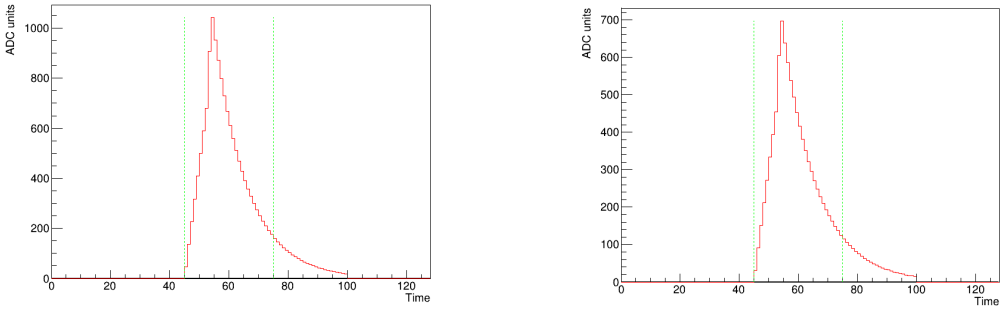

(**a**) Left SiPM. (**b**) Right SiPM.

Figure 17. Simulated waveforms for left and right SiPMs, depicted in red, with the integral window [45, 75] highlighted in green.

To investigate the effect of coating reflectivity on the photopeak position, a simulation was performed using 1% of the light yield, instead of the actual light yield of LYSO, which

is about 33,200 ph/MeV [9], to speed up our simulation. We examined various coating reflectivities (0.981, 0.987, 0.990, 0.995, 0.997, 0.998, 0.999) and recorded the total number of photons forming the photopeak from both the left and right SiPMs at each reflectivity. As shown in Figure 19, the photopeak position decreases as the reflectivity decreases. For example, the photopeak position for the 0.999 reflectivity coating is the highest, around 205, while the lowest mean, corresponding to the 0.981 reflectivity, is around 130. This demonstrates a decrease in the mean value of approximately 36.6%. This function with the sigma over mean from Figure 19 shows the sensitivity of coating reflectivity in this setup. A 5% change in the photopeak mean is already a measurable quantity; therefore, the refractive index can be measured with a resolution of about 0.1% in the range of reflectivity between 0.995 and 0.999.

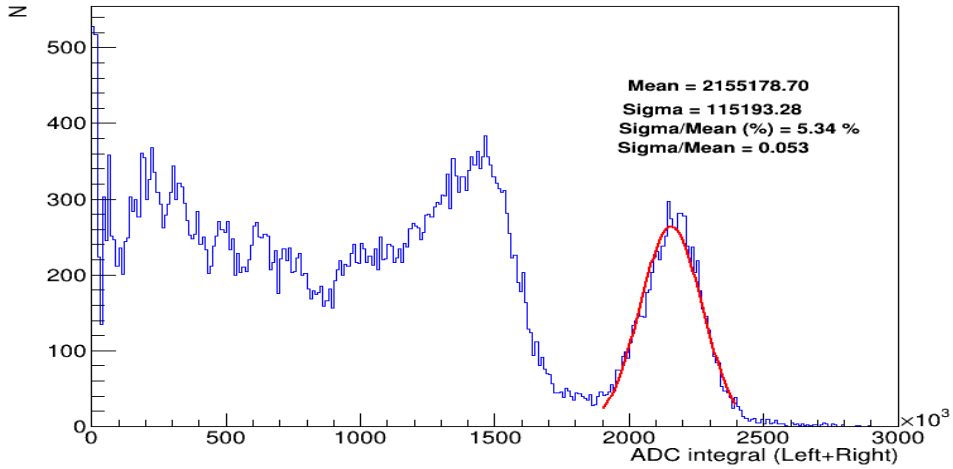

Figure 18. ADC integral for the summation of left and right SiPM, shown in blue, with the Gaussian fitting of the photopeak depicted in red. From the fitting, the sigma per mean is approximately 10%.

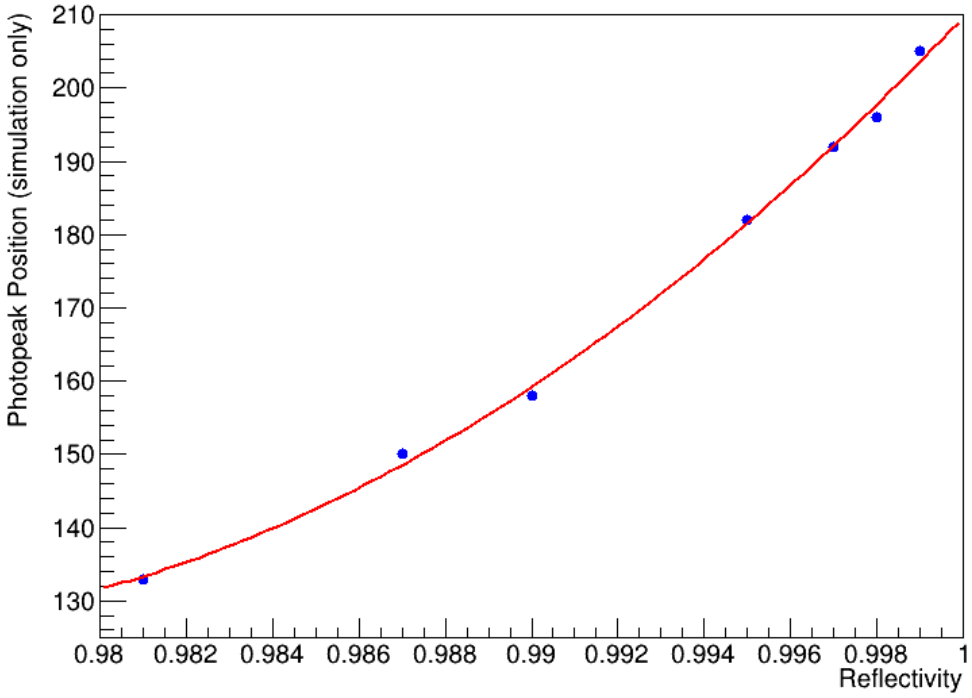

Figure 19. Photopeak position dependence on reflectivity of coating.

5. Discussion

With accurate, high-data-capacity electronics and the use of simulation techniques, the quality control of SiPM-based detectors can be performed with a short test and simulation. If, as in this case, this measurement can be based on the results of a previous test (SiPM: breakdown voltage, gain; LYSO: absorption length; coating: refractive index), a good estimate can be obtained for all relevant parameters, including the quality of the bonding, which cannot be measured by other tests.

Author Contributions: D.B. developed the readout process, the GUI, the data analysis and the GEANT4 simulation. S.O. worked on the FPGA framework. B.G. desigend the PCBs and implemented the FPGA code. B.U. did the source test. A.M. worked on the GEANT4 analysis. All authors have read and agreed to the published version of the manuscript.

Funding: This research was funded by the National Research, Development and Innovation Office (NKFIH) OTKA 131991, OTKA 143540 and NKFIH 2021-4.1.2-NEMZ_KI-2022-00022.

Data Availability Statement: The original contributions presented in the study are included in the article, further inquiries can be directed to the corresponding author.

Conflicts of Interest: The authors declare no conflicts of interest.

Abbreviations

The following abbreviations are used in this manuscript:

ADC	Analog-to-Digital Converter
APD	Avalanche Photodiode
ASIC	Application-Specific Integrated Circuit
BGO	Bismuth Germanate
CERN	Conseil Européen pour la Recherche Nucléaire, European Organisation for Nuclear Research
DAQ	data acquisition
GEANT4	Geometry ANd Tracking, CERN simulation framework for particle interaction
LIDAR	Light Detection And Ranging
LYSO	Lutetium Yttrium Oxyorthosilicate
MSPS	Megasamples Per Second
MRI	Magnetic Resonance Imaging
PCB	Printed Circuit Board
PET	Positron Emission Tomography
PMT	Photomultiplier Tube
PDE	Photon Detection Efficiency
SiPM	Silicon Photomultiplier
YSO	Yttrium OrthoSilicate
FPGA	Field-Programmable Gate Array

References

1. CMS Collaboration. A MIP Timing Detector for the CMS Phase-2 Upgrade. CERN Document Server. Available online: https://cds.cern.ch/record/2667167/files/CMS-TDR-020.pdf (accessed on 4 October 2023).
2. Santanastasio, F. Precision Timing in the CMS MTD Barrel Timing Layer with Crystal Bars and SiPMs. *IEEE Trans. Nucl. Sci.* **2020**, *67*, 2105–2110. [CrossRef]
3. Willeke, F.; Beebe-Wang, J. *Electron Ion Collider Conceptual Design Report 2021*; U.S. Department of Energy: Washington, DC, USA, 2021. [CrossRef]
4. Khalek, R.A.; Accardi, A.; Adam, J.; Adamiak, D.; Akers, W.; Albaladejo, M.; Al-bataineh, A.; Alexeev, M.G.; Ameli, F.; Antonioli, P.; et al. Science Requirements and Detector Concepts for the Electron-Ion Collider: EIC Yellow Report. *Nucl. Phys. A* **2022**, *1026*, 122447. [CrossRef]
5. CMS Collaboration. Phase 1 upgrade of the CMS Hadron Barrel Calorimeter. *Nucl. Instruments Methods Phys. Res. Sect. Accel. Spectrometers Detect. Assoc. Equip.* **2022**, *1042*, 167389. [CrossRef]
6. Yokoyama, M.; Minamino, A.; Gomi, S.; Ieki, K.; Nagai, N.; Nakaya, T.; Nitta, K.; Orme, D.; Otani, M.; Murakami, T.; et al. Performance of multi-pixel photon counters for the T2K near detectors. *Nucl. Instrum. Methods Phys. Res. Sect. Accel. Spectrometer Detect. Assoc. Equip.* **2010**, *622*, 567–573. [CrossRef]

7. The CALICE Collaboration. Construction and commissioning of the CALICE analog hadron calorimeter prototype. *Nucl. Instrum. Methods Phys. Res. Sect. Accel. Spectrometers Detect. Assoc. Equip.* **2019**, *926*, 85–100.
8. Brun, R.; Rademakers, F.; Panacek, S. ROOT, an object oriented data analysis framework. *Nucl. Instrum. Methods Phys. Res. A* **1997**, *389*, 81–86. [CrossRef]
9. Luxium Solutions. LYSO Scintillation Crystal. Available online: https://www.luxiumsolutions.com/radiation-detection-scintillators/crystal-scintillators/lyso-scintillation-crystals (accessed on 3 July 2024).
10. GEANT4 Collaboration. GEANT4: A Simulation Toolkit. Available online: https://geant4.web.cern.ch (accessed on 3 July 2024).
11. Agostinelli, S.; Allison, J.; Amako, K.; Apostolakis, J.; Araujo, H.; Arce, P.; Asai, M.; Axen, D.; Banerjee, S.; Barrand, G.; et al. Geant4—A simulation toolkit. *Nucl. Instrum. Methods Phys. Res. A* **2003**, *506*, 250–303. [CrossRef]
12. Lucchini, M.; on behalf of the CMS Collaboration. Development of the CMS MIP timing detector. *Nucl. Instrum. Methods Phys. Res. A* **2020**, *958*, 162090. [CrossRef]